Track-Level-Compensation Look-Up Table Improves Antenna Pointing Precision

W. Gawronski,[1] F. Baher,[1] and E. Gama[1]

This article presents the improvement of the beam-waveguide antenna pointing accuracy due to the implementation of the track-level-compensation look-up table. It presents the development of the table, from the measurements of the inclinometer tilts to the processing of the measurement data and the determination of the three-axis alidade rotations. The table consists of three axis rotations of the alidade as a function of the azimuth position. The article also presents the equations to determine the elevation and cross-elevation errors of the antenna as a function of the alidade rotations and the antenna azimuth and elevation positions. The table performance was verified using radio beam pointing data. The pointing error decreased from 4.5 mdeg to 1.4 mdeg in elevation and from 14.5 mdeg to 3.1 mdeg in cross-elevation.

I. Introduction

The Deep Space Station 25 (DSS 25) antenna shown in Fig. 1 is one of NASA's Deep Space Network beam-waveguide (BWG) antennas. At 34 GHz (Ka-band) operation, it is necessary to be able to track with a pointing accuracy of 2-mdeg root-mean-square (rms). Repeatable pointing errors of several millidegrees of magnitude have been observed during the BWG antenna calibration measurements. The systematic errors of order 4 and lower are eliminated using the antenna pointing model. However, repeatable pointing errors of higher order are out of reach of the model. The most prominent high-order systematic errors are the ones caused by the uneven azimuth track. The track is shown in Fig. 2. Manufacturing and installation tolerances, as well as gaps between the segments of the track, are the sources of the pointing errors that reach over 14-mdeg peak-to-peak magnitude, as reported in [1,2].

This article presents a continuation of the investigations and measurements of the pointing errors caused by the azimuth-track-level unevenness that were presented in [1] and [2], and it presents the implementation results. Track-level-compensation (TLC) look-up tables were created for the DSS 25, DSS 26, DSS 34, and DSS 55 antennas. To date, the most complete and detailed results were obtained for the DSS 25 and DSS 55 antennas. In this article, for brevity of presentation, we present the DSS 25 antenna results only.

---

[1] Communications Ground Systems Section.

The research described in this publication was carried out by the Jet Propulsion Laboratory, California Institute of Technology, under a contract with the National Aeronautics and Space Administration.

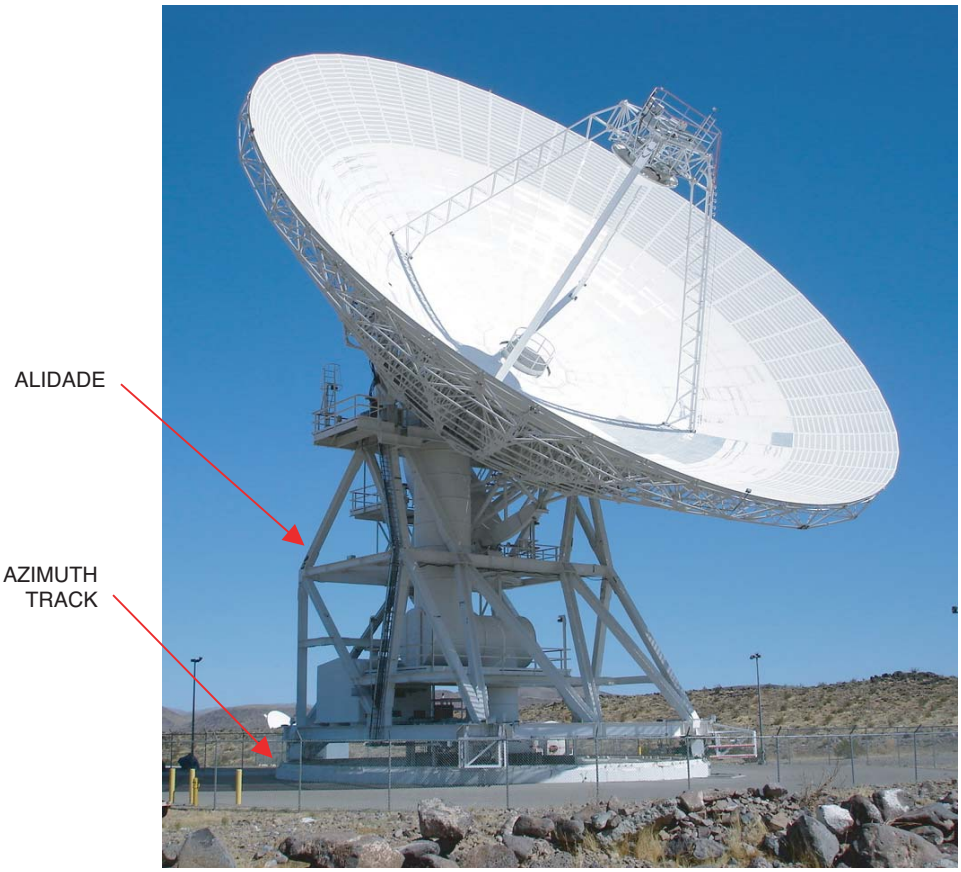

Fig. 1. The DSS 25 antenna.

The James Clerk Maxwell Telescope [5,6] and the 34-meter Kashima antenna [7] use inclinometers to perform track profile measurements to overcome possible systematic errors. However, the results have not been published. Track-level-unevenness compensation is planned for the Sardinia Radio Telescope [3]. A Green Bank Telescope memorandum [8] reports on pointing errors due to the azimuth-track-level unevenness; it has been reported that [9, pp. 2–3], "In the antenna engineering and operations area work on the Green Bank Telescope azimuth track was seen as most important." Inclinometers also were used for the thermal deformation of the Institut de Radioastronomie Millimétrique (IRAM) telescope [4].

II. Inclinometer Data Collection and Processing

TLC system hardware consists of four inclinometers, an interface assembly, and an industrial PC computer. Four digital inclinometers, model D711 of Applied Geomechanics, are mounted on the antenna. The inclinometers are located on the alidade, as shown in Fig. 3. Each inclinometer measures tilt in two axes, denoted "x" and "y." The manufacturer describes the inclinometer rotation as tilts. Note that x-axis tilt is equivalent to y-axis rotation, and vice versa; refer to Fig. 4.

Inclinometer data are collected while the antenna moves at a constant azimuth-axis rate of 0.05 deg/s. Due to environmental disturbances, the inclinometer data are extremely noisy. Take for example the x-axis movement of inclinometer 1, shown in Fig. 5. The unfiltered data are represented by the gray line. Using a zero-phase filter to prevent filtering delay, the data are smoothed, as represented by the red line.

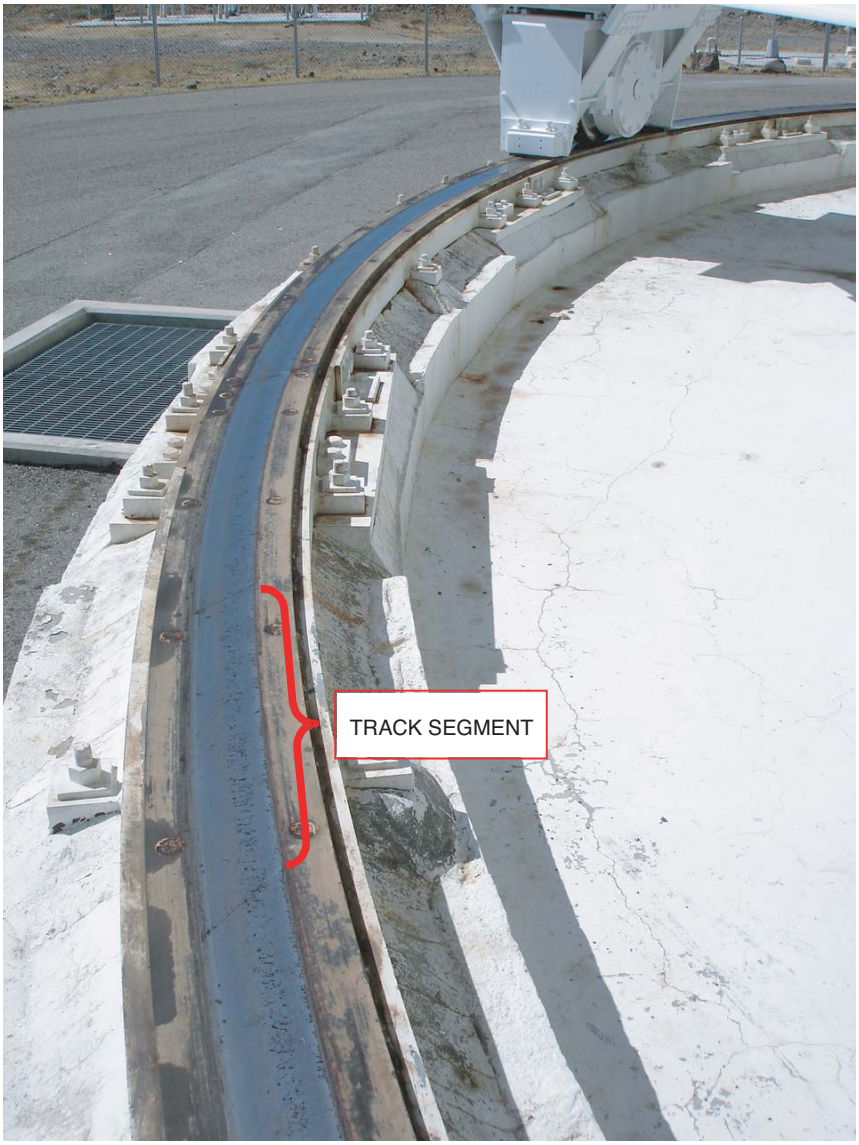

Fig. 2. The DSS 25 antenna's azimuth track.

The additional processing included the removal of the azimuth-axis tilt from the data. The tilt is present in the inclinometer data as harmonic functions in the x- and y-axes, of period 360 deg; see Figs. 6(a) and 6(b). The best-fit algorithm applied to the DSS 25 antenna resulted in a tilt of 3.45-mdeg magnitude and 310.64-deg phase. The x-axis movement of inclinometer 1 after the tilt removal is shown in Figs. 6(a) and 6(b) (red line).

The azimuth track is assembled from 16 rail segments. When the antenna rotates in azimuth, two wheels cross the gaps between the segments simultaneously, and the remaining two cross, also simultaneously, at a different azimuth position. Figure 7 shows the correlation between the inclinometer tilts and the locations of the gaps between the track segments that the wheels are crossing (red lines mark one pair of crossing wheels and blue dotted lines the second pair). The locations of the gaps correspond to the peaks of the tilt measurements.

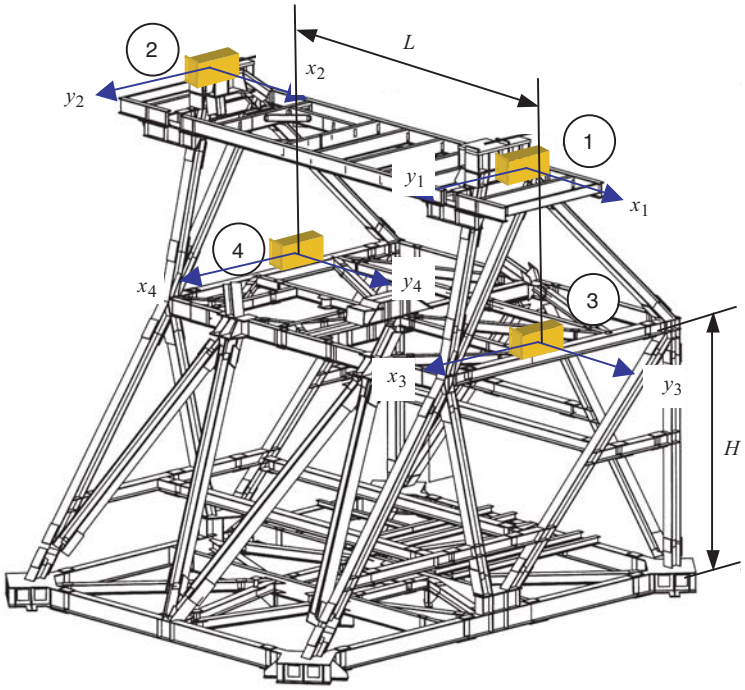

Fig. 3. The location of the inclinometers at the alidade.

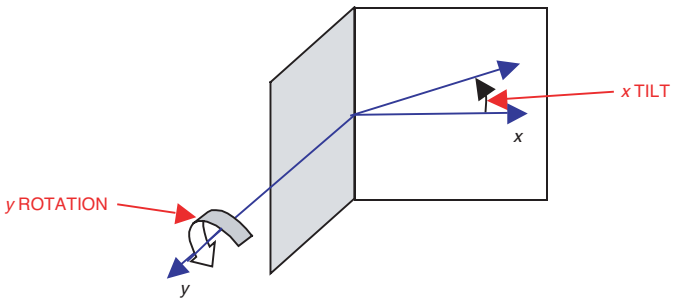

Fig. 4. The x-axis tilt is a rotation with respect to the y-axis.

III. Creating the TLC Table

The TLC look-up table consists of X, Y, and Z rotations of the alidade, as shown in Fig. 8. They are obtained from the inclinometer tilts, as shown in [1] and [2]—namely, a rotation with respect to the antenna x-axis, denoted X, is a rotation with respect to the antenna elevation axis. It is measured as the y-tilt of the second inclinometer (α_{2y}):

$$X = \alpha_{2y} \tag{1}$$

The Y rotation is a tilt of the elevation axis. It is an average of the x-tilts of inclinometers 1 and 2—that is,

$$Y = 0.5(\alpha_{1x} + \alpha_{2x}) \tag{2}$$

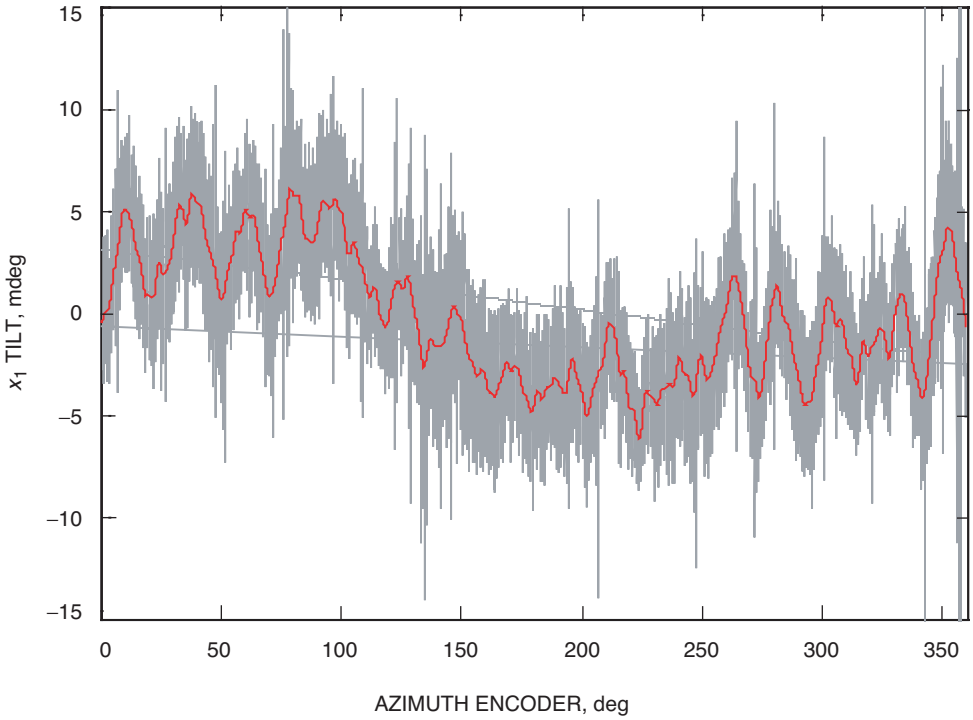

Fig. 5. The raw inclinometer data (gray line) and the filtered data (red line).

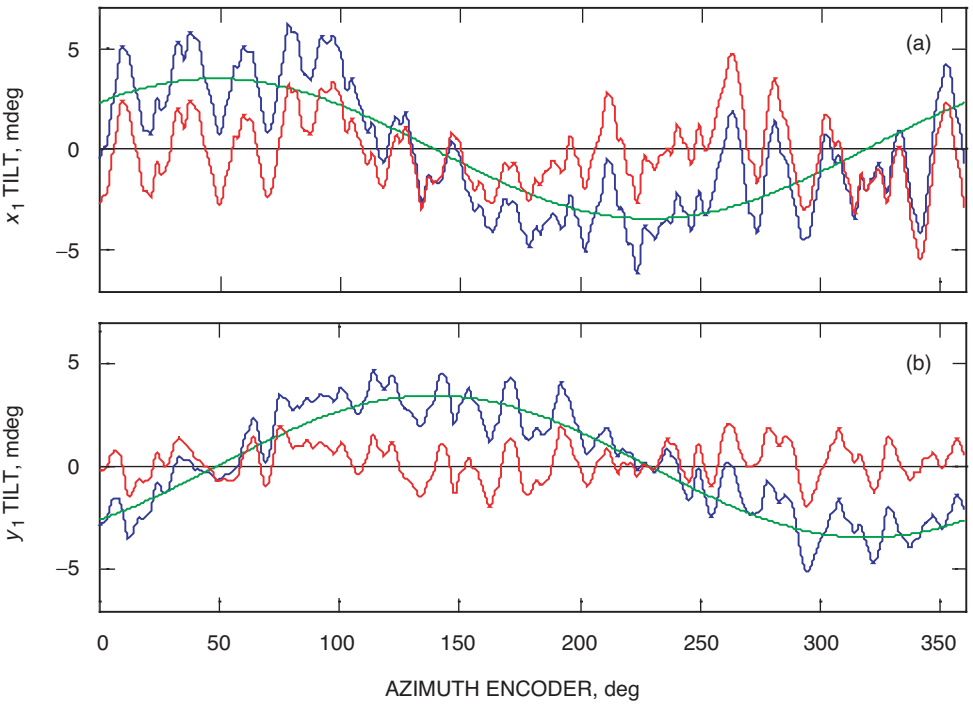

Fig. 6. Removing the azimuth axis tilt from the inclinometer data: (a) x-tilt of the first inclinometer and (b) y-tilt of the first inclinometer. (Blue line = inclinometer data; green line = inclinometer tilt caused by the azimuth axis tilt; red line = inclinometer data after azimuth axis tilt removal.)

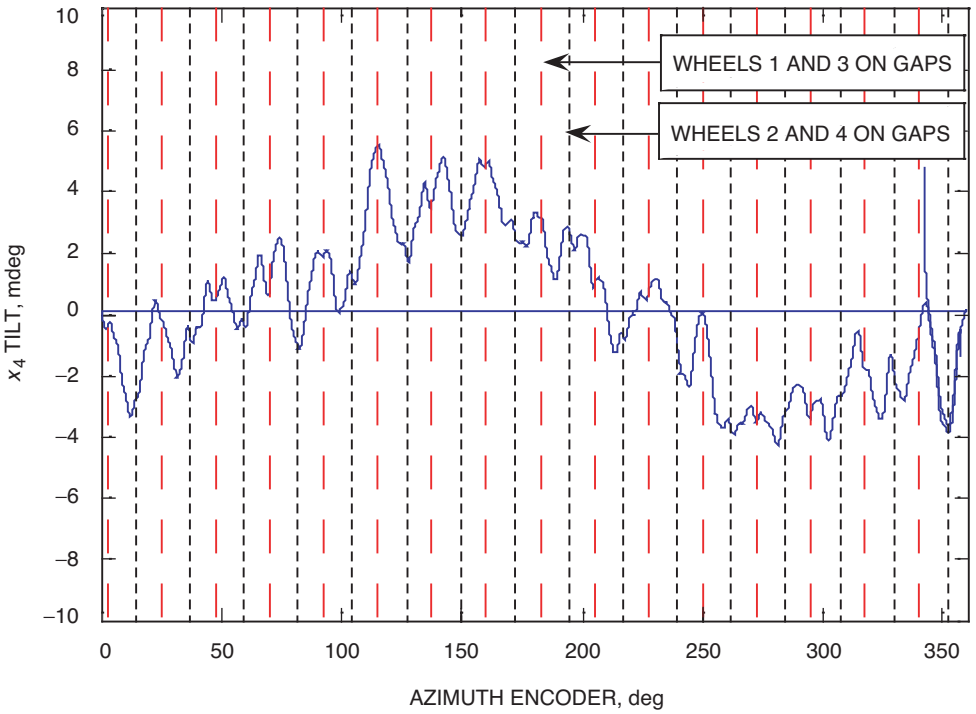

Fig. 7. Correlation between the peaks of the inclinometer tilts and the locations of the gaps between the track segments that the wheels are crossing (red lines mark one pair of crossing wheels, and black dotted lines mark the second pair).

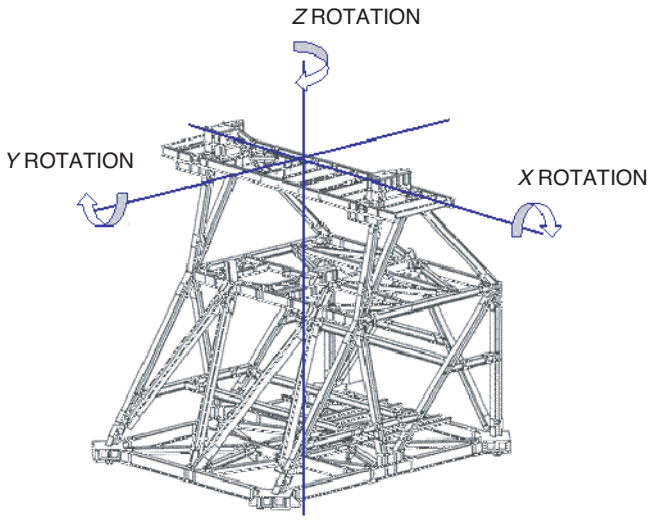

Fig. 8. *X*, *Y*, and *Z* rotations of the alidade.

The Z rotation of the alidade is a twist of the alidade, and it is not directly measured by inclinometers. It is determined from x-tilts of inclinometers 3 and 4, as follows. From Fig. 9, which represents a view from the top of the alidade, we have

$$Z = \frac{d_3 - d_4}{L} \tag{3}$$

where d_3 and d_4 are horizontal displacements of the locations of inclinometers 3 and 4, and $L = 12.396$ m is the distance between the two inclinometers. The displacements d_3 and d_4 are determined from the tilts of inclinometers 3 and 4, respectively, by assuming that the horizontal displacement of the alidade side due to azimuth-track unevenness is caused predominantly by the rigid-body motion of each side of the alidade, as shown in Fig. 10. This assumption was checked with the finite-element model of the alidade (see [1,2]), giving a 93 percent accuracy in estimation of displacements d_3 and d_4. It was confirmed by comparison of the rotations of the inclinometers located at the bottom, middle, and top of the alidade. The rigid-body angle is measured as the x-tilt of inclinometers 3 and 4 (denoted as α_{3x} and α_{4x}, respectively); therefore,

$$d_3 = H\alpha_{3x} \tag{4a}$$

and

$$d_4 = H\alpha_{4x} \tag{4b}$$

where H is the height at which the inclinometers are located and $H = 9.292$ m. Introducing Eq. (4) to Eq. (3), we obtain

$$Z = \frac{H}{L}(\alpha_{3x} - \alpha_{4x}) \tag{5}$$

where H is the alidade height and L is the distance between inclinometers 1 and 2. Since for the BWG antennas $L = 12.396$ m, the ratio is $H/L = 0.75$; therefore,

$$Z = 0.75(\alpha_{3x} - \alpha_{4x}) \tag{6}$$

The X, Y, and Z alidade rotations obtained from the inclinometer data, for azimuth angles varied from 0 to 360 deg and for a 0.1-deg azimuth angle sample size, are shown in Fig. 11. The plots show that the X rotation (the elevation correction) is comparatively small and that the largest is the Z rotation. It will be shown later that the Z rotation is compensated for by the azimuth encoder, and hence it is not an uncorrected part of pointing error.

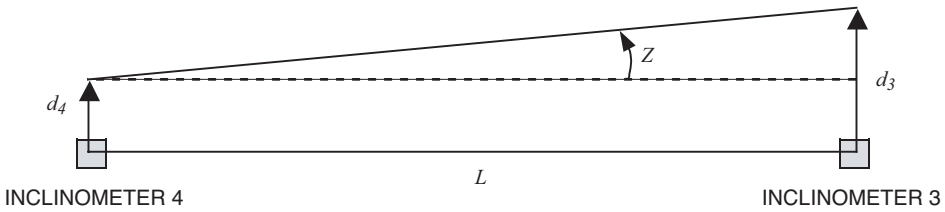

Fig. 9. Top view of inclinometers 3 and 4.

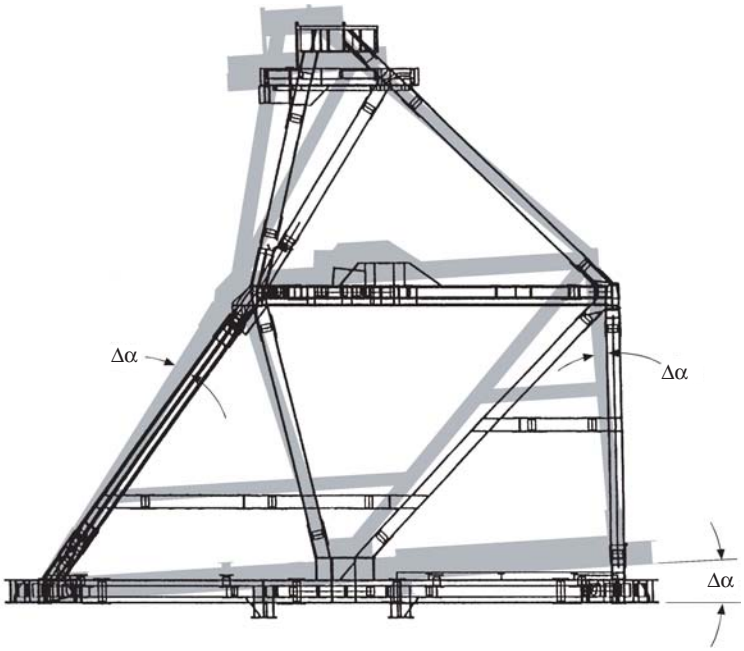

Fig. 10. Rigid body rotation of the alidade side.

IV. Comparing TLC Tables from 1998 and 2005

For the DSS 25 antenna, the look-up table was measured in 1998 and again in 2005. It is interesting to compare the results, which may indicate the wear of the track. The results are shown in Fig. 12: 1998 (red line) and 2005 (blue line). One can see slightly increased antenna tilt and a slightly different track pattern, but the plots indicate that over 7 years the track was quite stable.

V. Determining Pointing Errors from the TLC Table

The antenna elevation error Δ_{EL} is simply determined as the alidade X rotation:

$$\Delta_{EL} = X \tag{7}$$

The cross-elevation error, Δ_{XEL}, depends on the antenna elevation position, EL. It depends also, as shown in Fig. 13, on the Y and Z rotations of the alidade:

$$\Delta_{XEL} = Z\cos(EL) - Y\sin(EL) \tag{8}$$

Z-rotation contributions are left out of the TLC table because this error is measurable by the azimuth encoder and, therefore, eliminated by the azimuth servo. The following experiment at the DSS 55 antenna was conducted to verify this hypothesis. The antenna dish was positioned at $EL = 30$ deg. A 1-mm-thick shim was placed on the azimuth track, as shown in Fig. 14. The antenna then was moved slowly with constant speed in azimuth over the shim. The same antenna movement was repeated when the shim was removed. The difference between the azimuth encoder readings with and without the shim was calculated. The whole process was repeated when the antenna dish was positioned at $EL = 75$ deg. The difference between the azimuth encoder readings with and without the shim is plotted in Fig. 15. It shows

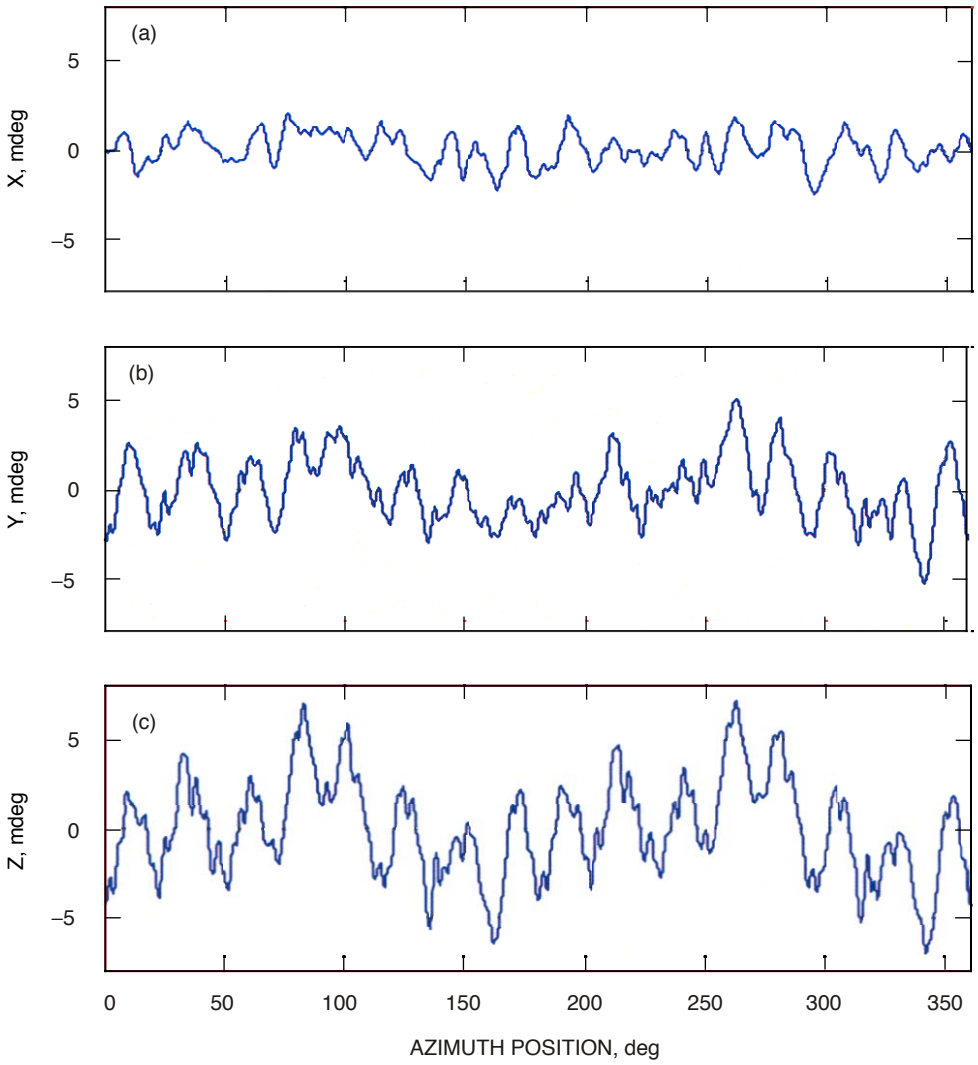

Fig. 11. The TLC look-up table of the DSS 25 antenna: (a) *X* alidade rotation, (b) *Y* alidade rotation, and (c) *Z* alidade rotation.

the azimuth position rising sharply (A) when the antenna is climbing the shim. But, the azimuth servo compensates for the shim disturbance, (B), and the azimuth position returns to the initial position (C). As a result, the antenna does not need correction in the z-axis, and the Z component of the TLC table will be zero.

Based on the above experiment, the following equation,

$$\Delta_{XEL} = -Y \sin(EL) \tag{9}$$

is the formula used for determination of the cross-elevation error.

VI. Antenna Pointing Improvement Using the TLC Table

The improvement of pointing accuracy when using the look-up table was evaluated using the radio-beam pointing data. The following beam-measurement techniques were used: boresight, monopulse, and

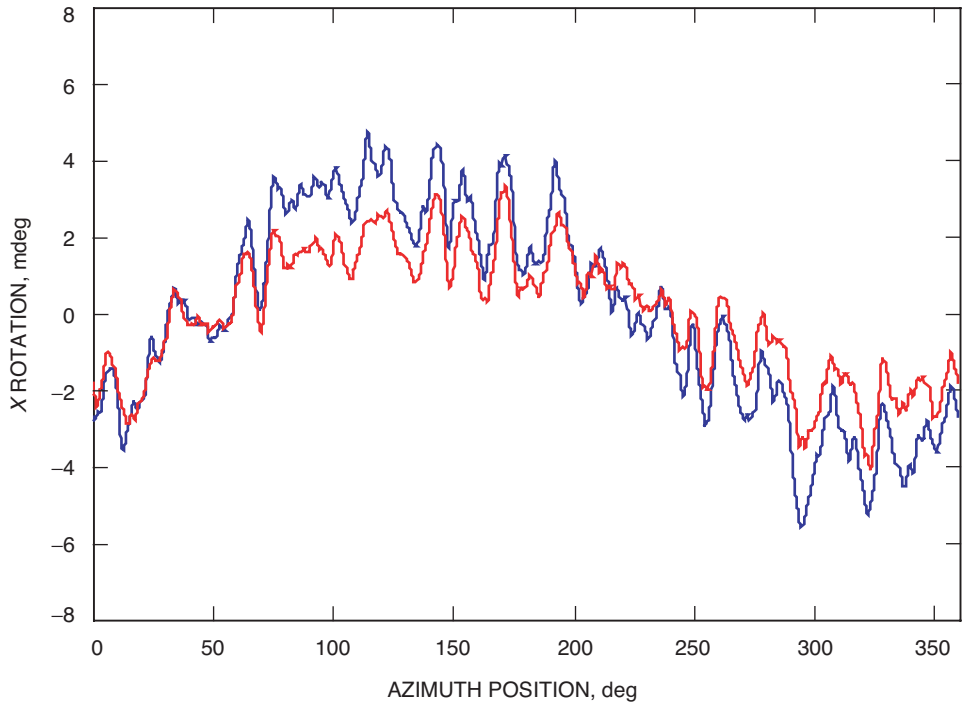

Fig. 12. The *X* rotation of the alidade of the DSS 25 antenna in 1998 (red line) and in 2005 (blue line). The latter shows larger axis tilt and increased "bumps."

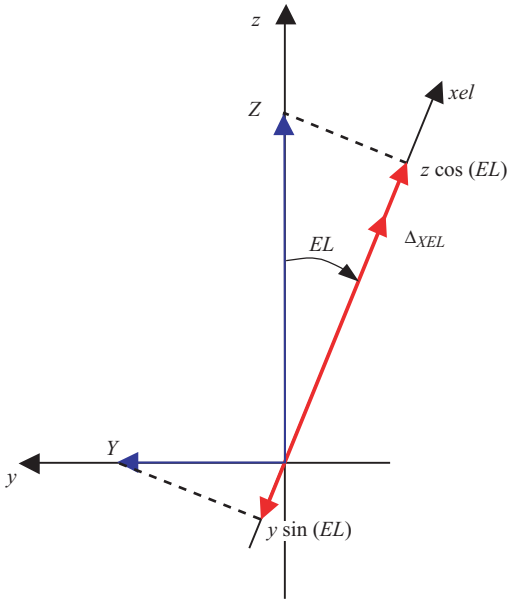

Fig. 13. The relationship between the cross-elevation error and the *X* and *Y* rotations of the alidade.

Fig. 14. The azimuth wheel crosses a 1-mm shim.

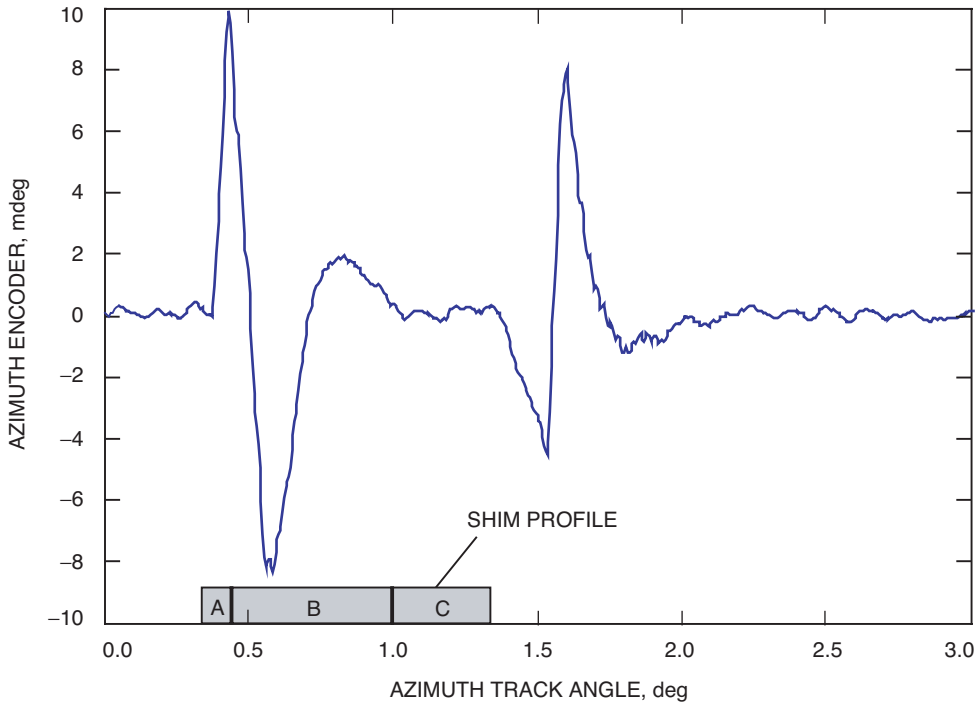

Fig. 15. The azimuth encoder reading difference when crossing the shim. "A" is a sharp rise in encoder reading at the beginning of the shim. "B" is the azimuth servo correction to the shim disturbance, and "C" is the stabilized azimuth position.

conscan. The data were measured either with the installed TLC table (TLC table on) or without the TLC table (TLC table off). Both methods are useful in the validation of the effectiveness of the TLC table. Namely, when the table is on, the pointing errors should be significantly smaller than the errors predicted from the TLC table (or the errors obtained for the same track with the TLC table off). When the table is off, the radio-beam pointing errors should match the errors predicted from the TLC table.

Figures 16(a) and 16(b) show measurements with the TLC table off. The measured elevation and cross-elevation beam pointing errors and the errors predicted by the look-up table coincide.

Next we investigate the elevation and cross-elevation pointing errors measured with the TLC table on. The tracking trajectory for which the radio-beam pointing data were taken is shown in Fig. 17. Note that the antenna is above $EL = 65$ deg for the azimuth position between 120 deg and 230 deg. The resulting pointing errors are shown in Fig. 18. The elevation pointing error is reduced to a random noise of standard deviation 0.38 mdeg (green line), while the TLC table predicts the error above 4 mdeg, from -2 to 2 mdeg (red line). The cross-elevation error, shown in Fig. 19, is predicted from the TLC table to vary by 7 mdeg, from -3 to 4 mdeg (red line). For $AZ < 120$ deg and for $AZ > 220$ deg, where the antenna is at an elevation position below 65 deg, the radio-beam data have random character and their standard deviation is 0.22 mdeg. For $120 < AZ < 230$ deg, where the antenna elevation position is above 65 deg, they are deterministic, ± 1.5 mdeg, peak-to-peak.

The reason for the appearance of the deterministic component of the cross-elevation error when the antenna elevation position is above 65 deg is not yet known. There are many possible reasons. One is that the Z rotation at the top of the alidade is different than the Z rotation at the encoder; therefore, it is not cancelled when the antenna is at a high elevation position. Another is the inaccurate estimation of the Y rotation. However, we would like to point out that the error caused by this fault is tolerable, because it is insignificant and short lived. The antenna stays above 65 deg in elevation for a rather short time, since at high elevation the azimuth rate is high. This is illustrated in Fig. 20, which presents the same cross-elevation error as in Fig. 18(b), but as a function of time rather than of azimuth position. One can see that the time above elevation 65 deg is less than 7 percent of the total tracking time.

Table 1 summarizes the antenna tracking accuracy with the TLC table on. The elevation pointing error decreased threefold, and the cross-elevation pointing error decreased almost fivefold.

VII. Conclusions

The article discussed the creation of the TLC look-up table from the inclinometer data and the determination of the elevation and cross-elevation errors from the look-up table. It also showed that the radio-beam pointing error significantly decreased from 4.5 mdeg to 1.4 mdeg in elevation and from 14.5 mdeg to 3.1 mdeg in cross-elevation when the look-up table was applied.

Future investigations will determine the source of the deterministic component of the cross-elevation error when the antenna elevation position is above 65 deg in order to eliminate completely the deterministic component of the pointing error.

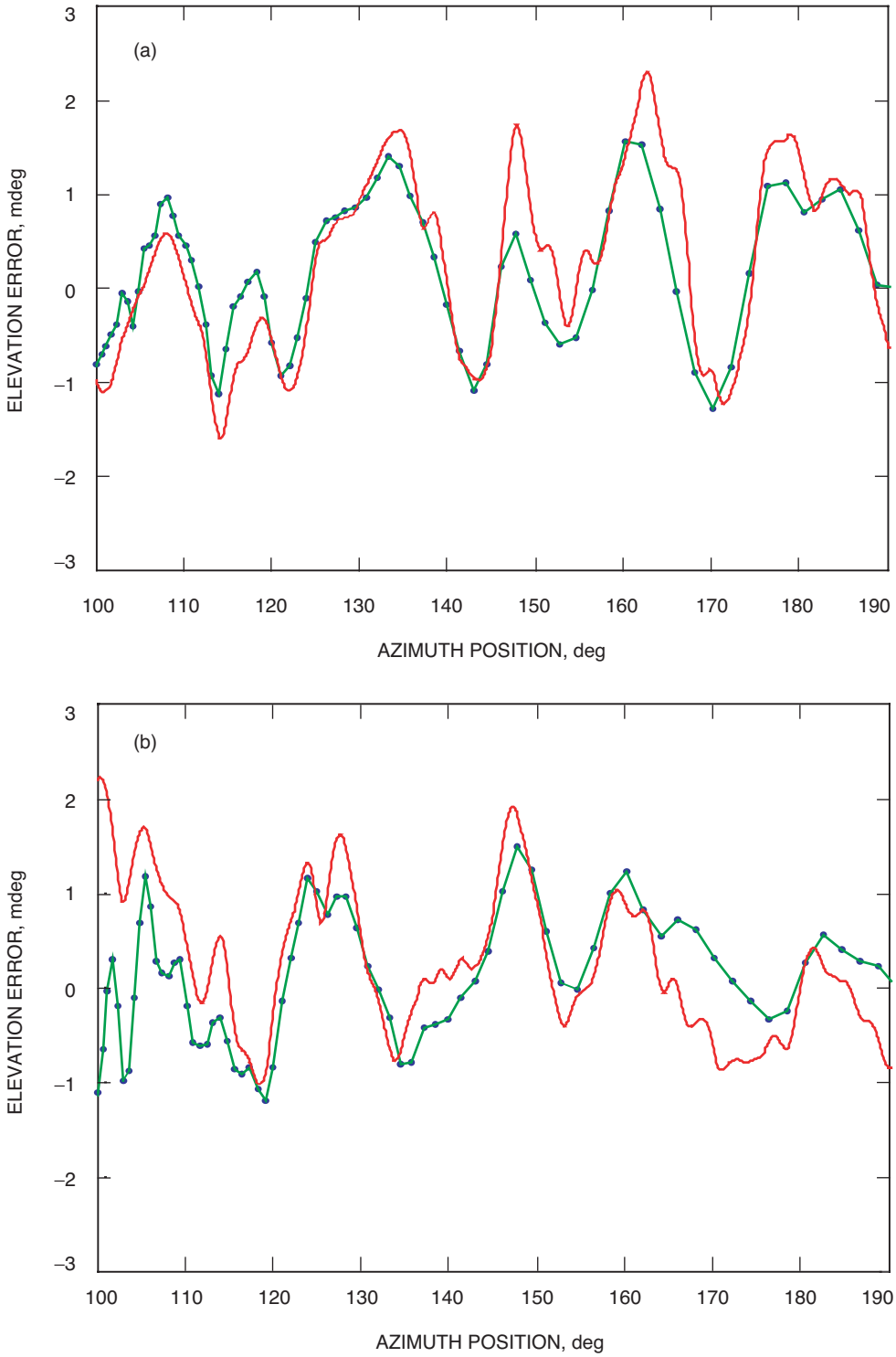

Fig. 16. The DSS 25 antenna pointing errors: (a) the elevation pointing error measured (green line with dots) and predicted from the TLC table (red line) and (b) the cross-elevation pointing error measured (green line with dots) and predicted from the TLC table (red line) with the z-correction added (*h* multiplier switched at *EL* = 65 deg).

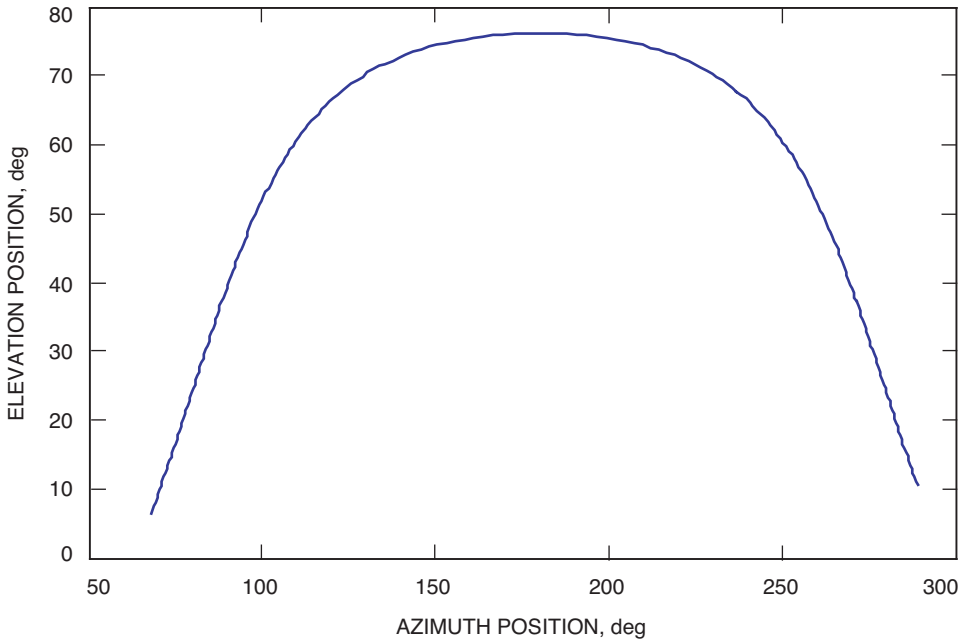

Fig. 17. Saturn trajectory on DOY 144, 2005.

Acknowledgments

Many people were involved in the measurements and validation of the TLC tables. The authors would like to acknowledge Graham Baines (Canberra Deep Space Communication Complex), Jesús Calvo (Madrid Deep Space Communication Complex), John Cucchissi (JPL), Manuel Franco (JPL), Tim Gregor (ITT, Goldstone Deep Space Communication Complex), David Muñoz (Madrid Deep Space Communication Complex), Pablo Perez (Madrid Deep Space Communication Complex), David Rochblatt (JPL), Ben Saldua (JPL), Manuel Vázquez (Madrid Deep Space Communication Complex), and Mike Wert (ITT, Pasadena) for collecting the pointing data and providing technical discussions. Special thanks to Watt Veruttipong (JPL) for his technical and managerial support.

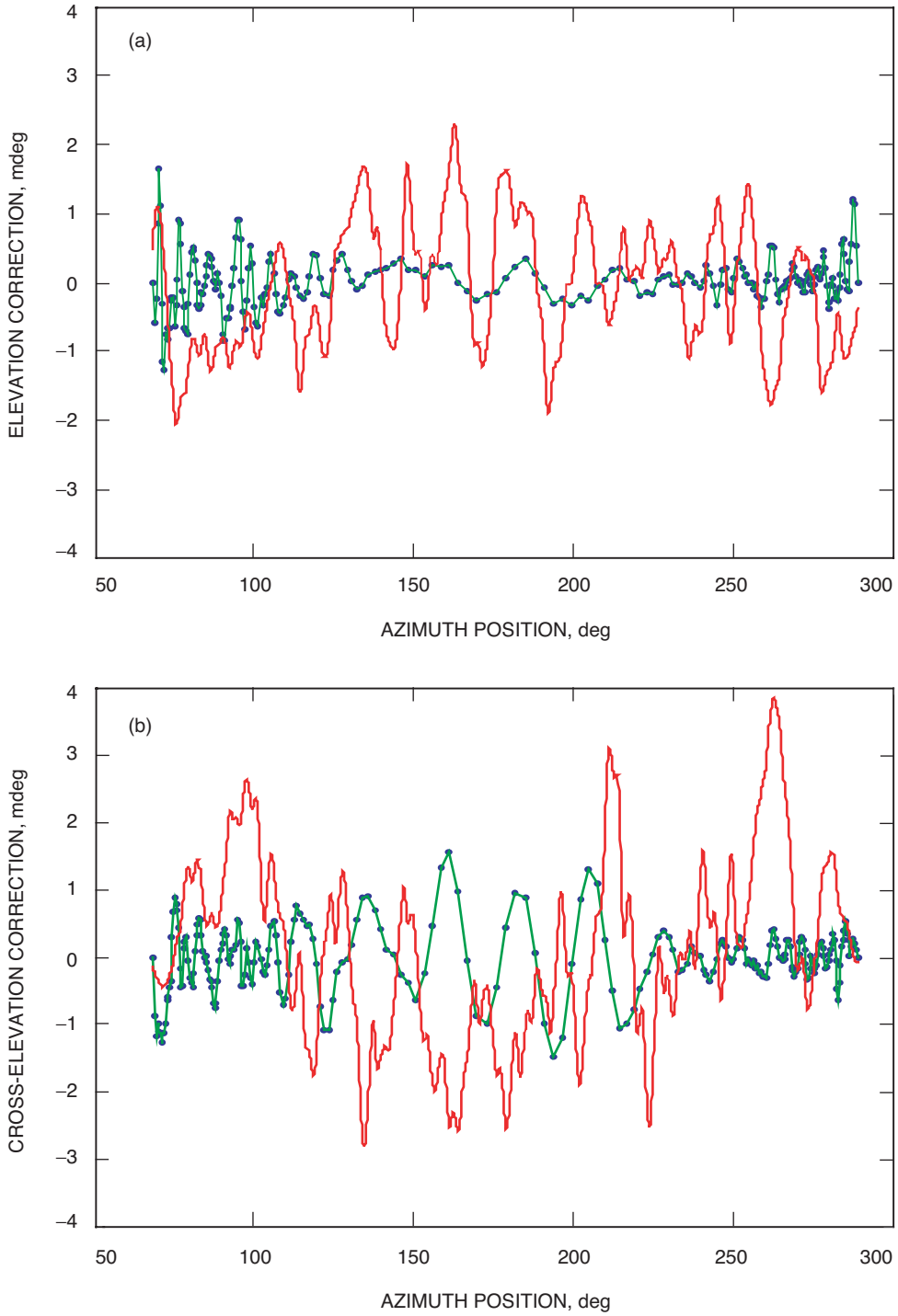

Fig. 18. The DSS 25 DOY 144 antenna pointing errors: (a) the elevation pointing error measured (green line with dots) and predicted from the TLC table (red line) and (b) the cross-elevation pointing error measured (green line with dots) and predicted from the TLC table (red line).

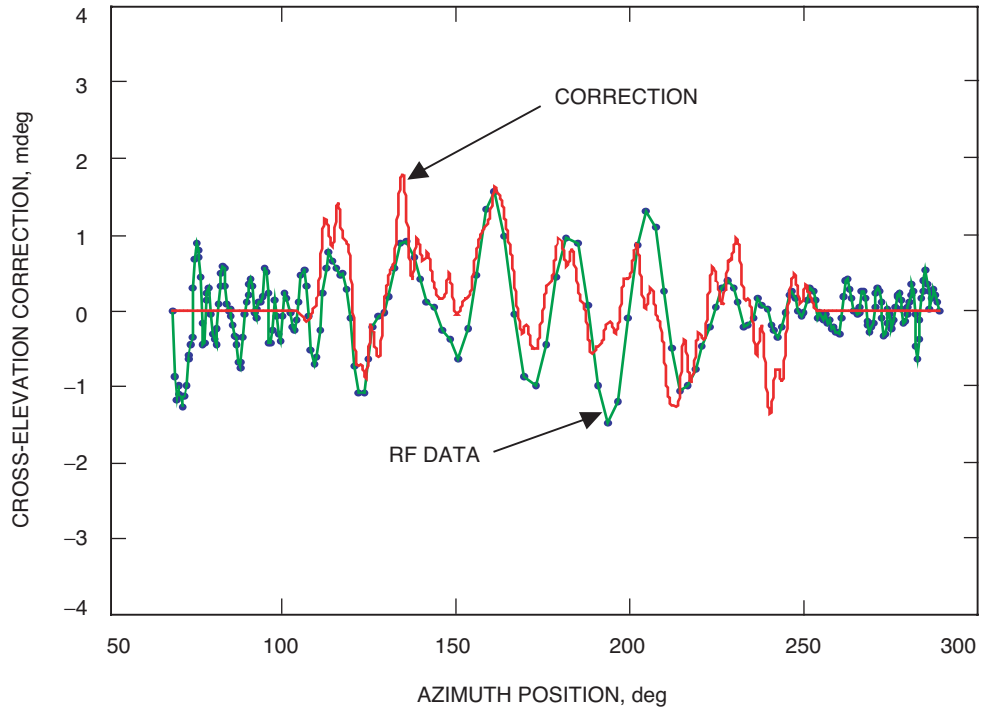

Fig. 19. The cross-elevation error measured (green line with dots) and predicted from the TLC table (red line) when the z-correction is added (*h* multiplier as in Fig. 7).

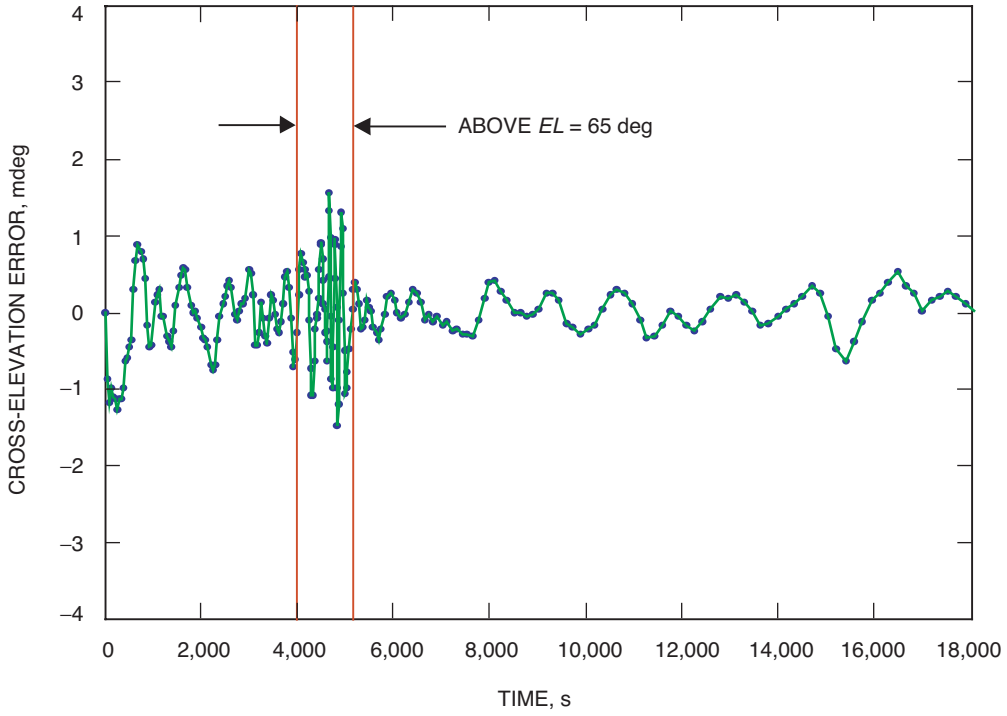

Fig. 20. The measured cross-elevation pointing error as a function of time.

Table 1. Peak-to-peak pointing errors (mdeg) of the DSS 25 antenna.

Pointing errors	Elevation error, mdeg	Cross-elevation error, mdeg
Without TLC table	4.5	14.1
With TLC table	1.4	3.1

References

[1] W. Gawronski, F. Baher, and O. Quintero, "Azimuth-Track-Level Compensation to Reduce Blind-Pointing Errors of the Beam-Waveguide Antennas," *The Telecommunications and Mission Operations Progress Report 42-139, July–September 1999*, Jet Propulsion Laboratory, Pasadena, California, pp. 1–18, November 15, 1999. http://ipnpr/progress_report/42-139/139D.pdf

[2] W. Gawronski, F. Baher, and O. Quintero, "Azimuth Track Level Compensation to Reduce Blind Pointing Errors of the Deep Space Network Antennas," *IEEE Antennas and Propagation Magazine*, vol. 42, no. 2, pp. 17–27, 2000.

[3] T. Pisanu, M. Morisani, C. Pernechele, F. Buffa, and G. Vargiu, "How to Improve the High Frequency Capabilities of SRT," *Proc. 7th European VLBI Network Symposium*, Toledo, Spain, 2004.

[4] A. Greve, M. Bremer, J. Penalver, P. Raffin, and D. Morris, "Improvement of the IRAM 30-m Telescope from Temperature Measurements and Finite Element Calculations," *IEEE Trans. Antennas and Propagation*, vol. 53, no. 2, pp. 851–860, 2005.

[5] http://www.jach.hawaii.edu/ets/mech/mech_recent.html

[6] http://www.jach.hawaii.edu/JCMT/telescope/pointing/20011006.html

[7] http://www2.nict.go.jp/ka/radioastro/tdc/news_19/pdf/okubo.pdf

[8] http://wwwlocal.gb.nrao.edu/ptcs/ptcspn/ptcspn40/AzTrackSpec.pdf

[9] http://www.nrao.edu/news/newsletters/nraonews94.pdf